Available online at www.sciencedirect.com
SCIENCE DIRECT®
PERGAMON
Solid State Communications 126 (2003) 93–101
solid state communications
www.elsevier.com/locate/ssc

Neutron scattering, magnetometry, and quantum Monte Carlo study of the randomly diluted spin-1/2 square-lattice Heisenberg antiferromagnet

O.P. Vajk[a], M. Greven[b,c,*], P.K. Mang[b], J.W. Lynn[d]

[a]*Department of Physics, Stanford University, Stanford, CA 94305, USA*
[b]*Department of Applied Physics, Stanford University, Stanford, CA 94305, USA*
[c]*Stanford Synchrotron Radiation Laboratory, Stanford University, Stanford, CA 94309, USA*
[d]*NIST Center for Neutron Research, National Institute of Standards and Technology, Gaithersburg, MD 20899, USA*

Received 7 August 2002; accepted 22 October 2002 by Y.J. Uemura

Abstract

We have successfully grown sizable single crystals of $La_2Cu_{1-z}(Zn,Mg)_zO_4$ with up to nearly half of the magnetic Cu sites replaced by non-magnetic Zn and Mg. Neutron scattering, SQUID magnetometry, and complementary quantum Monte Carlo (QMC) simulations demonstrate that this material is an excellent model system for the study of site percolation of the square-lattice Heisenberg antiferromagnet (SLHAF) in the quantum-spin limit $S = 1/2$. Carefully oxygen-reduced samples exhibit Néel order up to the percolation threshold for site dilution, $z_p \approx 40.7\%$. For $z > 10\%$, the material exhibits a low-temperature tetragonal (LTT) structural phase, with a transition temperature that increases linearly with doping. Above $z \approx 25\%$, Néel order occurs in the LTT phase. Up to at least $z = 35\%$, the Néel temperature $T_N(z)$ of the experimental system corresponds to the temperature at which QMC indicates that the spin correlations for the nearest-neighbor $S = 1/2$ SLHAF have grown to approximately 100 lattice constants. Neutron scattering measurements of the static structure factor in the paramagnetic regime allow the determination of the two-dimensional spin correlations, which are found to be in excellent quantitative agreement with QMC over a wide common temperature and doping range. Neutron scattering and QMC results for the temperature dependence of the static structure factor amplitude $S(\pi,\pi)$ are in good agreement as well. As the concentration of non-magnetic sites is increased, the magnetic correlation length $\xi(T,z)$ crosses over from an exponential dependence on ρ_s/T to power-law behavior in the temperature regime studied. Fits to a heuristic cross-over form for $\xi(T,z)$ allow an estimate of the spin stiffness, $\rho_s = \rho_s(z)$, which approaches zero at $z = z_p$. The combined experimental and numerical data presented here provide valuable quantitative information for tests of theories of the randomly diluted $S = 1/2$ SLHAF.

PACS: 75.10.Jm; 75.10.Nr; 75.40.Cx; 75.40.Mg; 73.43.Nq

Keywords: A. Insulators; B. Crystal growth; D. Phase transitions; D. Spin dynamics; E. Neutron scattering

The discovery of high-temperature superconductivity in charge-carrier doped La_2CuO_4 has stimulated an enormous interest in the properties of low-dimensional quantum magnets. The main structural building block of La_2CuO_4 and of related Mott insulators is a square lattice of Cu^{2+} spin-1/2 magnetic ions that experience a strong nearest-neighbor (NN) antiferromagnetic superexchange ($J \approx 1550$ K) mediated by intervening oxygens. Apart from small correction terms (such as anisotropies and a three-dimensional coupling), which lead to Néel order at a non-zero temperature, the magnetic degrees of freedom of these

* Corresponding author. Address: T. H. Geballe Laboratory for Advanced Materials, Stanford University, Stanford, CA 94305-4045, USA. Tel.: +1-650-725-8978; fax: +1-650-724-3681.
E-mail address: greven@stanford.edu (M. Greven).

0038-1098/03/$ - see front matter © 2003 Elsevier Science Ltd. All rights reserved.
PII: S0038-1098(02)00708-1

CuO_2 sheets are well-described by the square-lattice Heisenberg Hamiltonian

$$\mathscr{H} = J \sum_{\langle i,j \rangle} \mathbf{S}_i \cdot \mathbf{S}_j, \tag{1}$$

where the sum is over NN sites, J is the antiferromagnetic Cu–O–Cu superexchange, and $\mathbf{S}_i$ is the $S = 1/2$ operator at the site i.

Extensive experimental [1–10], quantum Monte Carlo (QMC) [11–13], and theoretical [14–24] efforts have led to a good understanding of the quantum many-body physics described by Eq. (1). The discrete Hamiltonian Eq. (1) has been mapped to a continuum quantum non-linear σ model (QNLσM), and it has been established that the NN square-lattice Heisenberg antiferromagnet (SLHAF) exhibits a broken-symmetry ground state (and renormalized classical behavior) rather than a quantum-disordered ground state even in the extreme quantum-spin limit of spin-1/2 [14]. Numerical and theoretical studies indicate that the quantum critical point separating these two ground states may be traversed, for example, upon the introduction of frustrating next-NN interactions [14,25] or by coupling two SLHAFs to form a bilayer [26]. Although the full spin Hamiltonian of La_2CuO_4 is believed to contain a frustrating next-NN exchange of about $0.05–0.10J$ [7,8,27], this is well below the value of $\approx 0.24J$ needed to disorder the system [25].

Quantum phase transitions in the presence of disorder are the subject of considerable current interest. Magnetic systems are often of particular value in this context, as the combined effects of quantum fluctuations and quenched disorder can be studied with various analytical and numerical methods. Furthermore, model magnets, if they can be found in nature, can serve as an important testing ground of theoretical predictions. A significant amount of theoretical and numerical effort has been devoted to the relatively simple one-dimensional [28,29] and two-dimensional [30,31] Ising model in a transverse field. For the $O(3)$ symmetric $S = 1/2$ SLHAF, the effects of a single impurity are well understood [32–34], but there are few theoretical results for finite impurity concentrations [35]. There have been suggestions that random site [30,36,37] and bond [38] dilution of the NN $S = 1/2$ SLHAF may lead to a non-trivial quantum phase transition. Extensive experimental results exist for $S = 5/2$ up to very high impurity concentrations [39], but results for the extreme quantum-spin limit of $S = 1/2$ have been limited to lower concentrations [5,40–48]. In studies of site-diluted $S = 5/2$ Heisenberg and Ising antiferromagnets [39,49], long-range order was found to disappear only above the percolation threshold $z_p \approx 40.725\%$ [50,51]. Earlier results for the Néel temperature of randomly diluted La_2CuO_4 extrapolate to zero temperature at concentrations well below the percolation threshold [5,40–47]. These results, along with theoretical predictions [30,36,37] and numerical studies [52], suggested the possible existence of a new quantum critical point at $z_{S=1/2} < z_p$. However, recent Monte Carlo simulations

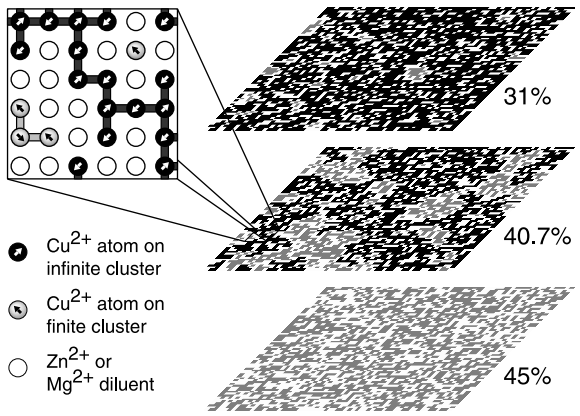

Fig. 1. Schematic of finite-sized sections of the infinite square lattice with random site dilution. Sites on the infinite cluster are shown in black, sites on finite disconnected clusters in grey, and diluents in white. At a concentration of 31%, most of the lattice is still connected. At 40.7%, just below the percolation threshold, much of the lattice is disconnected, but there is still a percolating cluster that spans the infinite lattice. Above the percolation threshold, all clusters are of finite size. The inset is a close-up view of the lattice, showing the role that magnetic Cu and non-magnetic Zn/Mg ions play in the experimental system.

[53–59] indicate that the site diluted NN $S = 1/2$ SLHAF remains ordered up to the percolation threshold. While the zero-temperature transition appears to be a classical percolation transition, the intermediate-temperature properties of the spin-1/2 system at $z = z_p$ seem to be controlled by the effective proximity to a new multicritical point [58,59].

Very recently, we have been able to show that $La_2Cu_{1-z}(Zn,Mg)_zO_4$ is a model material for the study of the effects of non-magnetic impurities in the $S = 1/2$ SLHAF up to and beyond the site percolation threshold [56]. Fig. 1 is a schematic of the randomly diluted CuO_2 sheets in $La_2Cu_{1-z}(Zn,Mg)_zO_4$, showing the geometric transition from an infinite connected cluster to finite disconnected clusters as the percolation threshold is traversed. We have also performed QMC simulations of the randomly diluted NN $S = 1/2$ SLHAF,

$$\mathscr{H} = J \sum_{\langle i,j \rangle} p_i p_j \mathbf{S}_i \cdot \mathbf{S}_j, \tag{2}$$

where $p_i = 1$ ($p_i = 0$) on magnetic (non-magnetic) sites. The experimental results for the static structure factor in the 2D correlated paramagnetic region agree remarkably well with our numerics [56], indicating that $La_2Cu_{1-z}(Zn,Mg)_zO_4$ is indeed a very good model system. The present paper outlines some aspects of these results in more detail.

1. Sample growth and characterization

A lack of stoichiometric samples at high non-magnetic

concentrations had limited earlier experimental work on randomly diluted La_2CuO_4. In previous studies of polycrystalline samples the concentration of non-magnetic ions was as high as 25% [47], significantly below the percolation threshold. Single crystal results had been limited even further, to $z \approx 15\%$ and below [5,44,46]. Furthermore, the excess oxygen typically found in as-grown samples introduces holes into the copper–oxygen sheets which frustrate the antiferromagnetism and quickly destroy magnetic order [60]. Differing values for $T_N(z)$ indicate that this problem had not been fully resolved [5,40–47].

We have successfully grown single crystals of $La_2Cu_{1-z}(Zn,Mg)_zO_4$ by the optical traveling-solvent floating-zone method. Zn^{2+} and Mg^{2+} are non-magnetic and have larger and smaller ionic radii, respectively, than Cu^{2+}. By jointly substituting Zn and Mg for Cu, we succeeded in growing samples up to and beyond the percolation threshold [56]. The Zn content of our samples is approximately 10%, while the Mg content varies. Typical single-grain sections are about 4 mm in diameter and 40 mm long. The composition of the samples was measured with electron probe microanalysis on sections cut from the ends of the crystals. Some crystals have small Cu/Zn/Mg concentration gradients along the length ($\Delta z = 1–2\%$), but all crystals are very uniform radially. The mosaic widths are very good, 15′ full width at half maximum (FWHM) or less, as measured by neutron diffraction. Samples were carefully annealed for 24 h at 900–950 °C in an Ar atmosphere to remove excess oxygen. Using SQUID magnetometry and neutron diffraction we checked that subsequent anneals do not further raise T_N, confirming that the first anneal was successful.

The neutron scattering measurements presented here were performed at the National Institute of Standards and Technology (NIST) Center for Neutron Research (NCNR), using the BT2 and BT9 thermal instruments and the SPINS cold neutron instrument.

2. Phase diagram

Near the Néel transition, the uniform susceptibility of $La_2Cu_{1-z}(Zn,Mg)_zO_4$ becomes coupled to the staggered susceptibility through the antisymmetric Dzyaloshinskii–Moriya term (not included in Eqs. (1) and (2)), and the uniform susceptibility perpendicular to the CuO_2 sheets increases to a cusp at T_N [46,61]. In order to determine the Néel temperature, small pieces, a few mm on each side, were cut from the larger crystals for magnetometry. Fig. 2(a) shows the uniform susceptibility for several samples measured with a SQUID magnetometer. Polycrystalline samples, with concentrations assumed to be equal to their nominal values, yielded similar results. At higher dilution levels, a large Curie-like component emerges [46], and the cusp at T_N becomes more difficult to distinguish.

Neutron diffraction measurements allow us to follow

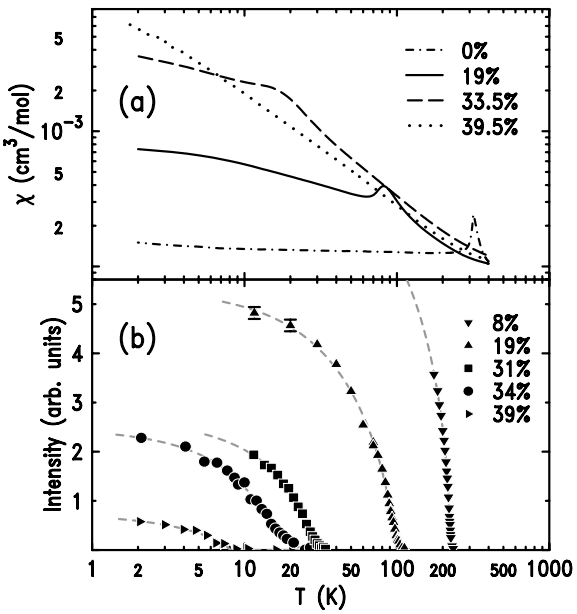

Fig. 2. Measurements of the Néel temperature $T_N(z)$ for several samples. (a) Magnetic susceptibility measured with a SQUID magnetometer with a 500 Oe field applied along the c axis. The susceptibility exhibits a cusp at T_N. At higher concentrations, a strong Curie-like component emerges, making the cusps more difficult to distinguish. (b) (1,0,0) magnetic Bragg peak intensity from neutron diffraction. A temperature-independent component, which is predominantly due to nuclear double scattering, has been subtracted. The lines represent fits for the magnetic order parameter squared, $\sim(T_N - T)^{2\beta}$ with $\beta \approx 0.30$, assuming a Gaussian distribution of T_N (typically $\approx$4 K) due to inhomogeneities present in the large samples used.

$T_N(z)$ at higher concentrations. The intensity at a magnetic Bragg reflection is proportional to the square of the staggered magnetic moment, and the doping dependence of the extracted ordered moment [56] agrees rather well with recent theoretical [35] and numerical [57] results for the NN SLHAF. Fig. 2(b) shows the temperature dependence of the scattering at the (1,0,0) magnetic reflection for several samples (we use orthorhombic (*Bmab*) notation throughout). The neutron diffraction results for T_N agree with SQUID measurements at low and intermediate concentrations and indicate that Néel order persists up to at least $z = 39\%$.

We typically observe an additional temperature-independent non-magnetic signal which was subtracted from the data in Fig. 2(b). This remnant signal is a combination of double scattering from the (1,0,2) and (0,0,2) nuclear Bragg reflections and a small $\lambda/2$ contamination due to nuclear scattering of higher-energy neutrons. The double-scattering component is strongly energy-dependent, and decreases at lower neutron energies. Neutrons with half the wavelength (and four times the energy) of the primary beam will also be diffracted by the monochromator. Such neutrons are filtered out with pyrolitic graphite on thermal instruments or berylium on SPINS, but small numbers

may still pass through if the filter is not sufficiently thick, giving rise to weak (2,0,0) nuclear Bragg scattering at the same angular position as the primary beam at the (1,0,0) magnetic peak.

The correction terms to Eqs. (1) and (2) are believed to include a small frustrating next-NN exchange [7,8,27], which might in principle become more important at higher concentrations, where T_N is relatively small, and lead to low-temperature spin-glass behavior. The associated spin freezing would be expected to lead to a momentum broadening of the magnetic peaks. Moreover, the observed transition temperature would depend on the probe frequency. We have tested for the possibility of low-temperature spin-glass physics and found in all samples that showed magnetic order (up to $z = 39\%$), that the width of the observed magnetic peaks remained resolution limited. Furthermore, we measured the temperature dependence of the magnetic scattering in a 35% diluted sample using incident neutron energies of 3.5, 5, and 13 meV, with FWHM energy resolutions ranging from 0.08 to 0.72 meV, as shown in Fig. 3. Since the transition temperature is independent of the neutron energy resolution over a relatively wide range of energies, we conclude that the observed behavior is a genuine Néel transition [62].

At high temperatures, pure La_2CuO_4 is in the so-called high-temperature tetragonal (HTT) phase (*I*4/*mmm*). Below about 530 K, the oxygen octahedra surrounding the copper ions tilt in a staggered fashion, creating an orthorhombic distortion of the CuO_2 planes and forming the low-temperature orthorhombic (LTO) phase (*Bmab*). In a 8% Zn-doped sample, we find that the HTT to LTO transition temperature increases to 577 K, but we have not followed this transition to higher concentrations, although previous experiments have found that it increases monotonically with both Zn and Mg doping [41]. Above $z = 10\%$, we discovered a second structural transition into a low-temperature tetragonal (LTT) phase ($P4_2/ncm$). Fig. 4 shows longitudinal scans through the (2,0,0) position measured by neutron diffraction above, at, and below the LTT transition temperature $T_{LTT} = 63(5)$ K for $z = 19\%$. The two peaks observed at higher temperature correspond to the (2,0,0) and (0,2,0) reflections. Both are observed in the same scan because of the presence of twin domains with different orthorhombic distortion directions. In the LTT phase, only one reflection is observed. The redistribution of intensity from the orthorhombic peaks to the tetragonal peak without a shift in the peak positions indicates that this is a first-order transition. We note, that the LTT phase has previously been observed in $(La,Ba)_2CuO_4$ [63] and $(La,Sr,Nd)_2CuO_4$ [64].

The magnetic and structural phase diagram obtained from SQUID magnetometry and neutron diffraction is shown in Fig. 5. Below $z \sim 20\%$, our data agree well with several previous results [5,45–47]. Above this concentration, we find that $T_N(z)$ deviates from a linear behavior, approaching zero only at the percolation threshold. Although random dilution weakens the tendency to order [56], it appears that quantum fluctuations are not strong enough to shift the critical point: $z_{S=1/2} = z_p$, within the uncertainty of our experiment.

The pure two-dimensional Heisenberg antiferromagnet described by Eq. (1) cannot exhibit long-range order at non-zero temperature. However, weak inter-plane couplings and anisotropies in $La_2Cu_{1-z}(Zn,Mg)_zO_4$ lead to Néel order at non-zero temperature approximately when $\alpha_{eff}\xi_{2D}^2 \approx 1$,

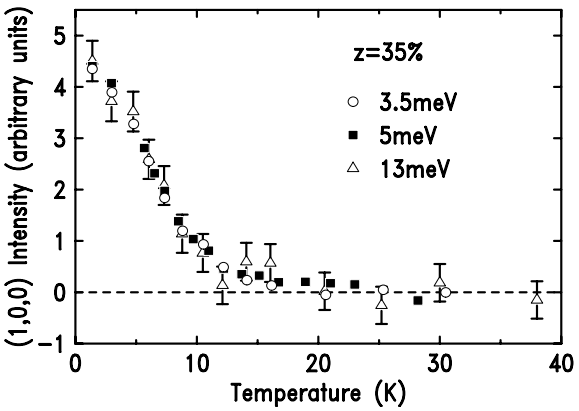

Fig. 3. Order parameter measurements performed on the 35% sample on the cold neutron instrument using neutron energies of 3.5, 5, and 13 meV. The corresponding energy resolutions range from 0.08 to 0.72 meV (FWHM). Even at very high concentrations close to the percolation threshold, the order parameter measurement remains independent of the energy resolution, indicating Néel rather than spin-glass order. A temperature-independent component of the signal, which is highly energy-dependent and predominantly due to double scattering involving the nuclear (1,0,2) and (0,0,2) reflections, has been subtracted from the data.

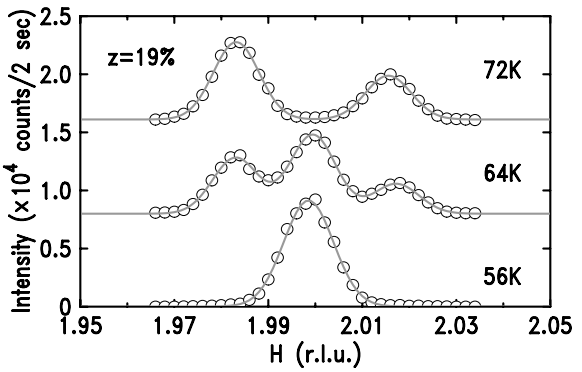

Fig. 4. Neutron diffraction measurements of the first-order structural phase transition from the orthorhombic to the low-temperature tetragonal phase at 19% dilution using 14.7 meV neutrons and collimations of 10′-27.5′-sample-23.7′-open. Scans are offset vertically, and lines indicate Gaussian fits. Above the transition, the longitudinal scans show a superposition of (2,0,0) and (0,2,0) peaks from different crystal domains. In the transition region, both phases coexist, partly because of the weakly first-order nature of the transition, and because of the small concentration gradient present in our samples. In the tetragonal phase, only one peak is observed.

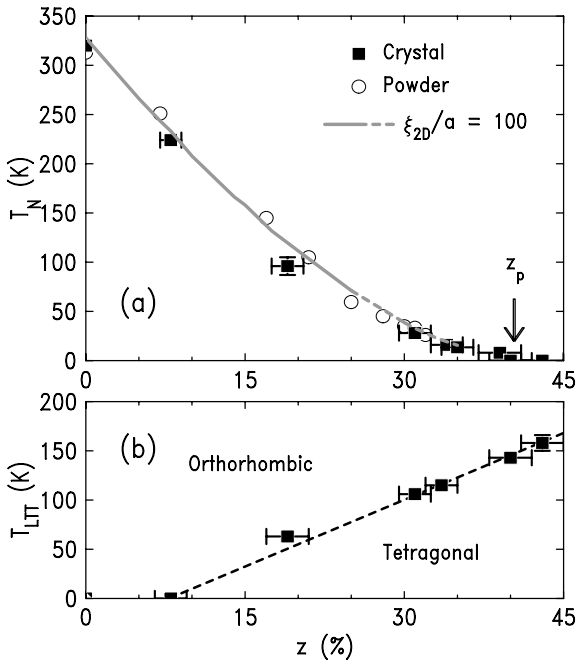

Fig. 5. Magnetic and structural phase diagram of $La_2Cu_{1-z}(Zn,Mg)_zO_4$. (a) Néel temperature vs. dilution. Single crystal results are from neutron measurements of the order parameter, powder results are from SQUID susceptibility measurements of polycrystalline samples. Our results up to $z = 25\%$ are in good agreement with previous work. The decrease of $T_N(z)$ at higher concentrations is not linear, but more gradual. Within the uncertainty of our experiment, $T_N(z)$ reaches zero at the percolation threshold, $z_p \approx 40.7\%$. (b) Structural transition temperature from orthorhombic to LTT phase, as measured by neutron diffraction. The doping dependence of the transition temperature is approximately linear, as indicated by the dashed line. We note that for $z > 10\%$ the Mg concentration of our samples was typically 10% while the Zn content varied.

where ξ_{2D} is the two-dimensional magnetic correlation length corresponding to Eq. (1) and α_{eff} is a suitable combination of the correction terms in the full spin Hamiltonian [7]. In pure La_2CuO_4, this occurs when $\xi_{2D} \approx 100a$, where a is the planar lattice constant [7]. Using QMC results for Eq. (2) (discussed in more detail below), we find remarkable agreement between the $\xi_{2D}/a = 100$ contour and $T_N(z)$ up to at least 35%. This is demonstrated in Fig. 5(a). The continuous line indicates direct numerical results for Eq. (2), while the dashed line results from an extrapolation of numerical data at higher temperatures. The full spin Hamiltonian describing $La_2Cu_{1-z}(Zn,Mg)_zO_4$ should depend on the details of the crystal structure. Above $z \approx 25\%$, Néel order occurs in the LTT phase. Nevertheless, $T_N(z)$ evolves smoothly with doping, and corresponds to $\xi_{2D}/a = 100$ from QMC for Eq. (2) even when $T_N < T_{LTT}$, as demonstrated in Fig. 5. Consequently, any changes with doping in the full spin Hamiltonian must be very subtle.

A non-zero next-NN exchange in $La_2Cu_{1-z}(Zn,Mg)_zO_4$ could shift the percolation threshold from the NN-only value of $z_p \approx 40.7\%$. Since the next-NN coupling in $La_2Cu_{1-z}(Zn,Mg)_zO_4$ is frustrating [8], it could, in principle, shift the critical point noticeably to a value below the percolation threshold (and lead to spin-glass physics, as discussed above) [39]. However, the value of the next-NN exchange is relatively small ($0.05-0.10J$) [8]. For the pure Hamiltonian Eq. (1), an additional frustrating next-NN coupling of $\approx 0.24J$ is needed to disorder the ground state [25]. We note that recent spin-wave measurements at the magnetic zone boundary suggest that the dominant further-neighbor interaction is not a next-NN exchange but a four-spin ring exchange [10], which does not extend connectivity beyond the NN percolation threshold.

3. Static structure factor measurement

We have systematically studied the static structure factor in the paramagnetic phase of $La_2Cu_{1-z}(Zn,Mg)_zO_4$, which allowed us to determine the instantaneous spin–spin correlation length $\xi(z,T)$. Above T_N, the 3D magnetic Bragg peaks become rods of 2D scattering. The static structure factor $S(q_{2D})$, where q_{2D} is the 2D momentum transfer component in the CuO_2 sheets relative to the 2D magnetic zone center, was measured with neutron scattering in two-axis, energy-integrating scans across these rods [7]. Fig. 6 shows representative data for two different samples. The measured peaks broaden as ξ decreases, both with increasing temperature and increasing dilution. Correlation lengths were obtained from fits to a single 2D Lorentzian

$$S(q_{2D}) = \frac{S(\pi,\pi)}{1 + q_{2D}^2\xi^2} \tag{3}$$

convoluted with the instrumental resolution. We note that well above T_N, the spin system is effectively isotropic. However, near T_N the anisotropy and 3D coupling terms in the full spin Hamiltonian lead to crossover physics. Our two-axis, energy-integrating experiment simultaneously measures both the in-plane and out-of-plane components of the static structure factor. Since our data do not allow for a line-shape analysis, we carried out fits to a single 2D Lorentzian.

The correlation lengths are plotted versus J/T in Fig. 7(a), and the static structure factor amplitude $S(\pi,\pi)$ is shown in Fig. 7(b). Temperature is scaled by $J = 135$ meV, the antiferromagnetic superexchange energy of the pure system [3,4]. The data are cut off above T_N by one standard deviation (≈ 4 K), as obtained from fits of the order parameter (Fig. 2(b)). From Fig. 7(a) it can be seen that dilution significantly decreases the rate at which correlations grow as the system is cooled. At high concentrations, $\xi(z,T)$ crosses over from exponential to power-law behavior. We note that the $z = 40(2)\%$ and $43(2)\%$ samples do not exhibit Néel order at 1.4 K ($J/T \approx 1100$), and the spin correlations appear to approach a constant zero-temperature value, as expected for $z > z_p$.

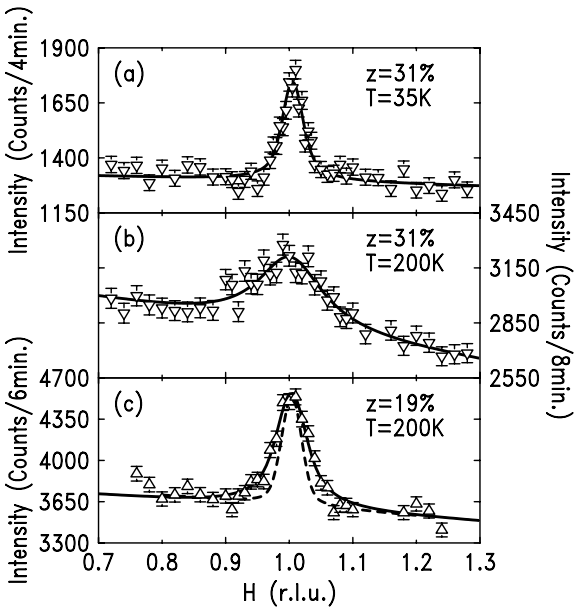

Fig. 6. Two-axis, energy-integrating measurements of the static structure factor taken with 30.5 meV incident neutron energy and horizontal collimations of 40′-27.5′-sample-23.7′. At 31% dilution (a) just above T_N and (b) well above T_N. (c) At 19% dilution, just above T_N. The dashed line in (c) indicates the instrumental resolution. Solid lines show fits to a 2D Lorentzian convoluted with the resolution, as discussed in the text.

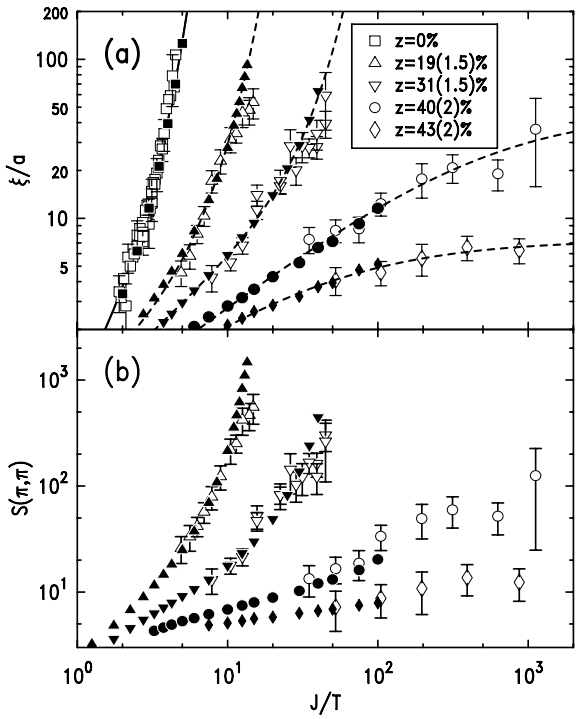

Fig. 7. (a) Spin–spin correlation lengths, in units of the lattice constant, versus inverse temperature, in units of the NN superexchange $J = 135$ meV of the pure system. Open symbols represent results from neutron scattering measurements of $La_2Cu_{1-z}(Zn,Mg)_zO_4$; filled symbols represent QMC data for $z = 0$, 20, 31, 41, and 46%. No adjustable parameters were used in the comparison. Experimental and QMC results for $z = 0$ are from previous work [7,13]. The dashed lines are fits to Eqs. (5) and (6), as described in the text, and the solid line is Eq. (4). (b) Static structure factor peak amplitude versus inverse temperature. Open symbols are neutron scattering results and filled symbols are from QMC, as above. Normalization between experimental and numerical results is discussed in the text.

4. Quantum Monte Carlo

In order to test the degree to which $La_2Cu_{1-z}(Zn,Mg)_zO_4$ is described by the randomly diluted NN Heisenberg Hamiltonian we have performed QMC simulations to calculate $\xi(z,T)$ for Eq. (2). We used a loop-cluster algorithm [56,65–67], with lattice sizes 10–20 times larger than the correlation length in order to avoid finite-size effects. We were able to simulate very large lattices of up to 1700×1700 sites, and to reach temperatures as low as $T = J/100$. Previous simulations were confined to very small lattices and high temperatures [52,68]. At each temperature and concentration, between 5 and 200 random configurations were averaged, with 10^4–10^5 measurements per configuration. The QMC results for $\xi(z,T)$, shown as filled symbols in Fig. 7(a), extend to higher temperatures and complement the experimental data. We find excellent quantitative agreement between the two up to the percolation threshold. We emphasize that this comparison contains no adjustable parameters, since J and a are known. Above the percolation threshold, the effective concentration of approximately 46% is slightly higher than the actual experimental value of 43(2)%. A possible origin for this might be a stronger relative influence of the next-NN term in the full spin Hamiltonian for $z > z_p$.

In Fig. 7(b), the static structure factor amplitude $S(\pi,\pi)$ from QMC (black symbols) is shown together with the experimental results. Unlike the correlation length, the measured amplitude also depends on experimental conditions, such as the effective illuminated sample volume and the neutron flux. Since the absolute value of $S(\pi,\pi)$ could not be determined with good accuracy, we have normalized the experimental data for each sample to match the respective numerical values. Note that the temperature scale is not adjustable. The temperature dependence of $S(\pi,\pi)$ can therefore still be compared between experiment and QMC, and we find good agreement.

5. Theory

The ground state of the pure NN SLHAF is ordered, but quantum fluctuations renormalize the spin-wave velocity, $c = 2\sqrt{2}SZ_c(S)Ja$, and spin-stiffness, $\rho_s = S^2Z_\rho(S)J$, from

their classical values (using units in which $g\mu_B = k_B = \hbar = 1$). For $S = 1/2$, the quantum renormalization factors Z_c and Z_ρ are known from theoretical and numerical studies, and $\xi(z = 0, T)$ is given by [14,15]

$$\frac{\xi}{a} = \frac{e}{8}\frac{c/a}{2\pi\rho_s} e^{2\pi\rho_s/T}\left[1 - \frac{1}{2}\left(\frac{T}{2\pi\rho_s}\right) + \mathcal{O}\left(\frac{T}{2\pi\rho_s}\right)^2\right] \quad (4)$$

with $c = 1.657Ja$ and $\rho_s = 0.18J$ [13]. Even though Eq. (4) is strictly valid only at asymptotically low temperatures [13–15,24], it agrees remarkably well with experiment [6–8] and numerics [12,13] in the range $2 < \xi/a < 200$ shown in Fig. 7(a).

The derivation of Eq. (4) involves mapping the discrete Hamiltonian Eq. (1) to the continuum quantum non-linear sigma model (QNLσM), and it assumes the existence of an ordered ground state and translational invariance. Random dilution breaks translational invariance and leads to defect rods in the Euclidian-time direction of the effective QNLσM. These rods break Lorentz invariance, and a QNLσM description may no longer be valid [14,35]. Furthermore, we can see from Fig. 7(a) that at higher concentrations the temperature dependence of $\xi(z,T)$ approaches power-law behavior. The modified form of Eq. (4)

$$\frac{\xi}{a} = \frac{e}{8}\frac{c/a}{2\pi\rho_s}\frac{e^{2\pi\rho_s/T}}{1 + (4\pi\rho_s/T)^{-\nu_T}} \quad (5)$$

with $\nu_T = 1$ has been suggested for disorder-free systems approaching a quantum critical point [69]. This crossover formula interpolates between Eq. (4) at $T < \rho_s$ and $\xi \sim 1/T$ as ρ_s approaches zero. Although recent studies indicate that $z = z_p$ is not a quantum critical point [57–59], random dilution reduces the spin stiffness and may be viewed as bringing the system closer to such a point in an extended parameter space.

In a classical picture, at $T = 0$, $z = z_p$ is a (geometric and thermal) multicritical point, and $\rho_s = 0$ as well as power-law behavior of $\xi(z_p,T)$ are expected. For the $S = 5/2$ system $Rb_2(Mn,Mg)F_4$ at and above the percolation threshold, the correlation length is well described by the form

$$\frac{1}{\xi(z,T)} = \frac{1}{\xi_0(z)} + \frac{1}{\xi_T(T)} \quad (6)$$

where $\xi_0(z)$ is the saturated zero-temperature length and $\xi_T(T) \sim T^{-\nu_T}$ [39]. At the percolation threshold, the thermal exponent of this $S = 5/2$ system was found to be $\nu_T = 0.90(5)$. A model based on the growth of 1D spin correlations along self-avoiding walks on the percolation cluster has been used successfully to describe these results for $Rb_2(Mn,Mg)F_4$ [70] without adjustable parameters. However, this model assumes classical spin chains, and the fact that we obtain a different exponent for $S = 1/2$ (see below) is therefore not surprising.

We have tested the extent to which Eqs. (4) and (5) describe our results by fitting the numerical data using $c(z)$ and $\rho_s(z)$ as adjustable parameters. We find that fits to Eq. (4) give a good description of $\xi(z,T)$, especially at low concentrations, and even at $z = 31\%$ for $\xi/a > 8$. However, the modified crossover form Eq. (5) even captures the high-temperature power-law behavior at higher concentrations, as shown in Fig. 7(a). Results for $c(z)$ and $\rho_s(z)$ from fits of Eq. (5), including dilution levels not shown in Fig. 7, are shown in Fig. 8. Using Eq. (4) results in large uncertainties for $c(z)$, but both $c(z)$ and $\rho_s(z)$ obtained using the two different forms agree within the errors. For the pure system, fits of QMC results [13] below $\xi/a = 200$ yield $2\pi\rho_s(0) = 1.18(1)J$ and $c(0) = 1.33(3)Ja$, about 4% higher and 20% lower, respectively, than the most accurate estimate [13]. For $z > z_p$, the combined QMC and experimental data were fit to Eq. (6). As can be seen in Fig. 7(a), our results are described well by this form. Overall, we obtain $\nu_T = 0.72(7)$ near the percolation threshold.

An attempt to combine percolation theory with the QNLσM model predicts for the spin stiffness [37]

$$\frac{\rho_s(z)}{\rho_s(0)} = A(z)\left[1 - \frac{\bar{g}(0)}{P_\infty(z)}\right]\frac{1}{1 - \bar{g}(0)}, \quad (7)$$

where $\bar{g}(0) = 0.685$ is the coupling constant corresponding to the NN $S = 1/2$ SLHAF at $z = 0$ [14], $A(z)$ is the bond dilution factor, and $P_\infty(z)$ is the probability of a site belonging to the infinite cluster of spins. $A(z)$ is well described up to $z \approx 37\%$ by $A(z) \approx 1 - \pi z + \pi z^2/2$ [71]. Up to $z \approx 20\%$, $P_\infty(z) \approx 1 - z$ [57] since at low concentrations there are very few separated clusters of spins so that $P_\infty(z)$ is mostly reduced from unity due to individual removed sites. Eq. (7), shown as a dotted line in Fig. 8, incorrectly predicts $\rho_s(z \approx 30\%) = 0$, and hence a quantum critical point well below the percolation threshold [37]. To our surprise, we find that substituting $1 + z$ for $1/P_\infty(z)$ quantitatively describes $\rho_s(z)/\rho_s(0)$ even at $z = 35\%$. This modified form of Eq. (7) is shown as a solid line in Fig. 8.

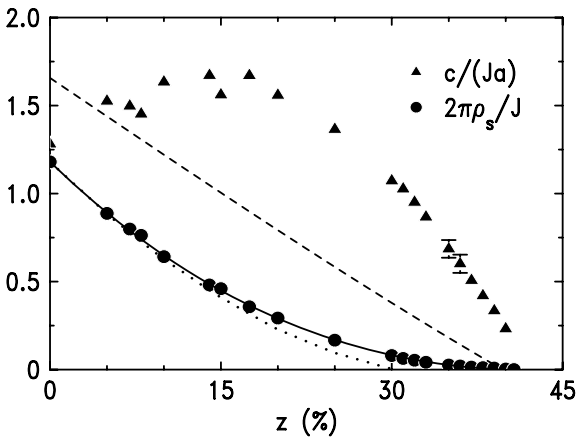

Fig. 8. Effective spin-wave velocity $c(z)$ and spin stiffness $2\pi\rho_s(z)$ as a function of non-magnetic concentration z extracted from fits to Monte Carlo results using the heuristic crossover form Eq. (5). Lines are discussed in the text.

This substitution matches the original expression at low concentrations and prevents the second term in Eq. (7) from going to zero below the percolation threshold. We note that Eq. (7) is a one-loop renormalization-group result, and (unknown) higher-order terms might perhaps improve agreement with our observations. Recent numerical finite-size scaling results for the spin stiffness give qualitatively similar results [57], but deviate from the unmodified form of Eq. (7) more quickly at lower concentrations. The expression for the spin-wave velocity corresponding to Eq. (7) is $c(z)/c(0) = A(z)(1 + z/2)$ [37], and is shown by the dashed line in Fig. 8. This expression does not match our QMC fit results, possibly for a number of reasons. Even at $z = 0$, a fit results in a 20% error in c [13]. Moreover, in the presence of random dilution, spin waves become strongly damped and the spin-wave velocity is not expected to be a well-defined quantity [35].

6. Discussion

Recent theoretical work for the randomly diluted $S = 1/2$ NN square-lattice Heisenberg antiferromagnet has produced exact results at low concentration [33] and led to predictions at intermediate concentrations [35,37]. Impurities may localize spin excitations and lead to a breakdown of the classical hydrodynamic description of excitations in terms of spin waves above a characteristic length scale [35]. Static properties such as the staggered magnetization and T_N, as well as the spin stiffness ρ_s, are expected to remain well defined. On the other hand, dynamic observables, such as the spin-wave velocity c, become ill-defined in this picture. As long as the ground state remains ordered, the low-temperature correlation length should still scale as $\xi \sim e^{2\pi\rho_s/T}$. This is consistent with our observation for $\xi(z,T)$ over a wide range of concentrations and temperatures, which we find to be well described by Eq. (4), and especially the heuristic crossover form Eq. (5).

Although the percolation transition for the 2D $S = 1/2$ Heisenberg antiferromagnet may be classical [57–59], recent QMC simulations of diluted bilayers indicate that the percolation threshold for the single layer system is very close to a new quantum multi-critical point in an extended parameter space [58,59]. Indeed, the dynamic critical exponent obtained in these studies is consistent with the thermal correlation length exponent $\nu_T \approx 0.7$ that we have found here. Therefore, in the temperature regime that we have studied, the properties of $La_2Cu_{1-z}(Zn,Mg)_zO_4$ near the percolation threshold appear to be controlled by this new critical point. Future inelastic neutron scattering measurements of the full dynamic structure factor should give further insight into this complex quantum many-body system.

Acknowledgements

O.P.V. and M.G. thank A. Aharony, A.H. Castro Neto, A.L. Chernyshev, A.W. Sandvik, and E.F. Shender for helpful discussions. The work at Stanford was supported by the US Department of Energy under contract nos. DE-FG03-99ER45773 and DE-AC03-76SF00515, by NSF CAREER Award no. DMR9985067, and by the A. P. Sloan Foundation.

References

[1] K.B. Lyons, P.A. Fleury, J.P. Remeika, A.S. Cooper, T.J. Negran, Phys. Rev. B 37 (1988) 2353.
[2] Y. Endoh, K. Yamada, R.J. Birgeneau, D.R. Gabbe, H.P. Jennsen, M. Kastner, Phys. Rev. B 37 (1988) 7443.
[3] G. Aeppli, S.M. Hayden, H.A. Mook, Z. Fisk, S.-W. Cheong, D. Rytz, J.P. Remeika, G.P. Espinosa, A.S. Cooper, Phys. Rev. Lett. 62 (1989) 2052.
[4] Y. Tokura, S. Koshihara, T. Arima, H. Takagi, S. Ishibashi, T. Ido, S. Uchida, Phys. Rev. B 41 (1990) 11657.
[5] B. Keimer, N. Belk, R.J. Birgeneau, A. Cassanho, C.Y. Chen, M. Greven, M.A. Kastner, A. Aharony, Y. Endoh, R.W. Erwin, G. Shirane, Phys. Rev. B 46 (1992) 14034.
[6] M. Greven, R.J. Birgeneau, Y. Endoh, M.A. Kastner, M. Matsuda, G. Shirane, Z. Phys. B 96 (1995) 465.
[7] R.J. Birgeneau, M. Greven, M.A. Kastner, Y.S. Lee, B.O. Wells, Phys. Rev. B 59 (1999) 13788.
[8] Y.J. Kim, R.J. Birgeneau, F.C. Chou, M. Greven, M.A. Kastner, Y.S. Lee, B.O. Wells, A. Aharony, O. Entin-Wohlman, I.Y. Korenblit, A.B. Harris, Phys. Rev. B 64 (2001) 024435.
[9] Y.J. Kim, R.J. Birgeneau, F.C. Chou, R.W. Erwin, M.A. Kastner, Phys. Rev. Lett. 86 (2001) 3144.
[10] R. Coldea, S.M. Hayden, G. Aeppli, T.G. Perring, C.D. Frost, T.E. Mason, S.W. Cheong, Z. Fisk, Phys. Rev. Lett. 86 (2001) 5377.
[11] M. Makivić, H.Q. Ding, Phys. Rev. B 43 (1991) 3562.
[12] J.-K. Kim, M. Troyer, Phys. Rev. Lett. 80 (1998) 2705.
[13] B.B. Beard, R.J. Birgeneau, M. Greven, U.-J. Wiese, Phys. Rev. Lett. 80 (1998) 1742.
[14] S. Chakravarty, B.I. Halperin, D.R. Nelson, Phys. Rev. B 39 (1989) 2344.
[15] P. Hasenfratz, F. Niedermayer, Phys. Lett. B 268 (1991) 231.
[16] S. Tyč, B.I. Halperin, S. Chakravarty, Phys. Rev. Lett 62 (1989) 835.
[17] R.R.P. Singh, Phys. Rev. B 39 (1989) 9760.
[18] J. Igarashi, Phys. Rev. B 46 (1992) 10763.
[19] A.V. Chubukov, S. Sachdev, J. Ye, Phys. Rev. B 49 (1994) 11919.
[20] C.J. Hamer, Z. Weihong, J. Oitmaa, Phys. Rev. B 50 (1994) 1994.
[21] N. Elstner, A. Sokol, R.R.P. Singh, M. Greven, R.J. Birgeneau, Phys. Rev. Lett. 75 (1995) 938.
[22] R.R.P. Singh, M.P. Gelfand, Phys. Rev. B 52 (1995) 15695.
[23] A. Cuccoli, V. Tognetti, R. Vaia, P. Verrucchi, Phys. Rev. B 56 (1997) 14456.
[24] P. Hasenfratz, Eur. Phys. J. B 13 (2000) 11.

[25] L. Siurakshina, D. Ihle, R. Hayn, Phys. Rev. B 64 (2001) 104406.
[26] P.V. Shevchenko, A.W. Sandvik, O.P. Sushkov, Phys. Rev. B 61 (2000) 3475.
[27] J.F. Annett, R.M. Martin, A.K. McMahan, S. Satpathy, Phys. Rev. B 40 (1989) 2620.
[28] A.P. Young, H. Rieger, Phys. Rev. B 53 (1996) 8486.
[29] S. Sachdev, A.P. Young, Phys. Rev. Lett. 78 (1997) 2220.
[30] T. Senthil, S. Sachdev, Phys. Rev. Lett. 77 (1996) 5292.
[31] H.-O. Heuer, Phys. Rev. B 45 (1992) 5691.
[32] A.W. Sandvik, E. Dagotto, D.J. Scalapino, Phys. Rev. B 56 (1997) 11701.
[33] S. Sachdev, C. Buragohain, M. Vojta, Science 286 (1999) 2479.
[34] M. Vojta, C. Buragohain, S. Sachdev, Phys. Rev. B 61 (2000) 15152.
[35] A.L. Chernyshev, Y.C. Chen, A.H.C. Neto, Phys. Rev. B. 65 (2002) 104407.
[36] C. Yasuda, A. Oguchi, J. Phys. Soc. Jpn 68 (1999) 2773.
[37] Y.-C. Chen, A.H. Castro Neto, Phys. Rev. B 61 (2000) R3772.
[38] A.W. Sandvik, M. Vekić, Phys. Rev. Lett. 74 (1995) 1226.
[39] R.J. Birgeneau, R.A. Cowley, G. Shirane, H. Yoshizawa, J. Stat. Phys. 34 (1984) 817 and references therein.
[40] A. Chakraborty, A.J. Epstein, M. Jarrel, E.M. McCarron, Phys. Rev. B 40 (1989) 5296.
[41] S.-W. Cheong, A.S. Cooper, L.W.J. Rupp, B. Batlogg, Phys. Rev. B 44 (1991) 9739.
[42] S.T. Ting, P. Pernambuco-Wise, J.E. Crow, E. Manousakis, Phys. Rev. B 46 (1992) 11772.
[43] R.L. Lichti, C. Boekema, J.C. Lam, D.W. Cooke, S.F.J. Cox, S.T. Ting, J.E. Crow, Physica C 180 (1991) 358.
[44] G. Cao, J.W. O'Reilly, J.E. Crow, L.R. Testardi, J. Appl. Phys. 75 (1994) 6595.
[45] M. Corti, A. Rigamonti, F. Tabak, P. Carretta, F. Licci, L. Raffo, Phys. Rev. B 52 (1995) 4226.
[46] K. Uchinokura, T. Ino, I. Terasaki, I. Tsukada, Physica B 205 (1995) 234.
[47] M. Hücker, V. Kataev, J. Pommer, J. Harras, A. Hosni, C. Pflitsch, R. Gross, B. Büchner, Phys. Rev. B 59 (1999) R725.
[48] S.J. Clarke, A. Harrison, J. Mag. Mag. Mater. 140 (1995) 1627.
[49] D.J. Breed, K. Gilijamse, J.W.E. Sterkenburg, A.R. Miedema, J. Appl. Phys. 41 (1970) 1267.
[50] D. Stauffer, A. Aharony, Introduction to Percolation Theory, 2nd ed. Taylor & Francis, Bristol, PA, 1994.
[51] M.E.J. Newman, R.M. Ziff, Phys. Rev. Lett. 85 (2000) 4104.
[52] S. Miyashita, J. Behre, S. Yamamoto, Computational Approaches in Condensed Matter Physics, Springer, Berlin, 1992, p. 97.
[53] K. Kato, S. Todo, K. Harada, N. Kawashima, S. Miyashita, H. Takayama, Phys. Rev. Lett. 84 (2000) 4204.
[54] S.S. Todo, H. Takayama, N. Kawashima, Phys. Rev. Lett. 86 (2001) 3210.
[55] C. Yasuda, S. Todo, M. Matsumoto, H. Takayama, Phys. Rev. B 64 (2001) 092405.
[56] O.P. Vajk, P.K. Mang, M. Greven, P. Gehring, J.W. Lynn, Science 295 (2002) 1691.
[57] A.W. Sandvik, Phys. Rev. B 66 (2002) 024418.
[58] A.W. Sandvik, Phys. Rev. Lett. 89 (2002) 177201.
[59] O.P. Vajk, M. Greven, Phys. Rev. Lett. 89 (2002) 177202.
[60] A. Aharony, R.J. Birgeneau, A. Coniglio, M.A. Kastner, H.E. Stanley, Phys. Rev. Lett. 60 (1988) 1330.
[61] T. Thio, T.R. Thurston, N.W. Preyer, P.J. Picone, M.A. Kastner, H.P. Jennsen, D.R. Gabbe, C.Y. Chen, R.J. Birgeneau, A. Aharony, Phys. Rev. B 38 (1988) 905.
[62] A.P. Murani, A. Heidemann, Phys. Rev. Lett. 41 (1978) 1402.
[63] J.D. Axe, A.H. Moudden, D. Hohlwein, D.E. Cox, K.M. Mohanty, A.R. Moodenbaugh, Y. Xu, Phys. Rev. Lett. 62 (1989) 2751.
[64] M.K. Crawford, R.L. Harlow, E.M. McCarron, W.E. Farneth, J.D. Axe, H. Chou, Q. Huang, Phys. Rev. B 44 (1991) 7749.
[65] H.G. Evertz, G. Lana, M. Marcu, Phys. Rev. Lett. 70 (1993) 875.
[66] U.-J. Wiese, H.-P. Ying, Z. Phys. B 93 (1994) 147.
[67] M. Greven, R.J. Birgeneau, Phys. Rev. Lett. 81 (1998) 1945.
[68] E. Manousakis, Phys. Rev. B 45 (1992) 7570.
[69] A.H. Castro Neto, D. Hone, Phys. Rev. Lett. 76 (1996) 2165.
[70] R.J. Birgenau, R.A. Cowley, G. Shirane, H.J. Guggenhein, Phys. Rev. Lett. 37 (1976) 940.
[71] A.B. Harris, S. Kirkpatrick, Phys. Rev. B 16 (1977) 542.